OPTICAL REVIEW Vol. 14, No. 4 (2007) 194–200

Measurement of Wavelength Dependence of Electro-Optic Coefficients r_{22} of Non-doped and 5% MgO-doped Congruent $LiNbO_3$ Crystals and 1.8% MgO-doped Quasi-stoichiometric $LiNbO_3$ Crystal by Multiple Reflection Interference Method

Kazuya YONEKURA, Lianhua JIN[1], and Kuniharu TAKIZAWA[1]

Department of Applied Physics, Faculty of Engineering, Seikei University, Musashino, Tokyo 180-8633, Japan
[1]*Department of Materials and Life Science, Faculty of Science and Technology, Seikei University, Musashino, Tokyo 180-8633, Japan*

(Received February 13, 2007; Accepted May 28, 2007)

The electro-optic coefficient r_{22} in the wavelength range from 409 to 1580 nm was measured for non-doped and 5% MgO-doped congruent $LiNbO_3$ crystals and 1.8% MgO-doped quasi-stoichiometric $LiNbO_3$ crystals in a simple optical system using a multiple reflection interference method capable of producing high-precision results without the application of antireflection film to the end faces of the crystal. The influence of the manufacturing errors of the electro-optic crystals was discussed on the measurement of the r_{22} coefficient. The experimental errors are less than approximately 0.5% in the wavelength range from 409 to 1064 nm and approximately 1% from 1340 to 1580 nm. It was further shown that polarizing of the laser along X axis resulted in highly accurate measurement of the r_{22} of $LiNbO_3$ crystals. © 2007 The Optical Society of Japan

Key words: $LiNbO_3$, electro-optic coefficient r_{22}, dispersion, interference measurement, measurement error

1. Introduction

Ferroelectric $LiNbO_3$ (LN) crystals have the following distinguishing qualities: (1) large electro-optic (EO) coefficients, (2) simple manufacturing of large crystal, (3) stability with respect to the environment due to deliquescence, (4) excellent workability, and (5) relatively low cost. Two large subgroups of LN crystals, congruent and stoichiometric,[1,2] are identified according to their composition. Furthermore, MgO-doped[3,4] and Fe-doped crystals have been developed in order to alter their original properties. Such LN crystals are used with a wide range of wavelengths such as blue light in holographic memory devices,[5–7] visible light in image correction devices,[8] and IR light in optical communication devices.[9,10] However, uniform measurements of the EO coefficients of LN crystals in the visible to IR domain are scarce, and there is a need to examine the broad-spectrum wavelength dependency of EO coefficients.

The methods for measuring the EO coefficients of LN crystals include the Mach–Zehnder[11,12] and Michelson[13,14] interference methods for phase measurement, as well as the Senarmont method[15,16] for retardation measurement. In those methods, when the light coherence length is two or more times that of the crystal, the multiple reflection within the crystal results in measurement errors. One of the authors has measured EO coefficient r_c consisting of r_{13} and r_{33} of LN crystals, and previously determined that the application of antireflection (AR) film to the end faces of the crystal is necessary for the purpose of precision measurement with coherence light.[17)]

The r_{22} of LN crystals is often measured for 632.8 nm, and reports of these, summarized in Table 1, are especially abundant. However, the wavelength dependence of r_{22} has not been sufficiently explored. Though Chirakadze *et al.*[18] determined the values of r_{22} for non-doped congruent LN (CLN) crystals in the 420–1150 nm wavelength, there is a possibility that their results were affected by multiple reflection.

Table 1. Absolute value of EO coefficient (r_{22}) of $LiNbO_3$ measured by various methods at 632.8 nm and at room temperature.

r_{22} (pm/V)	Reference
6.8	11
6.7	24, 25
6.4	16, 18, 26
6.3	27
6.54	Present result

The authors previously minimized the measurement errors resulting from multiple reflection by analyzing its influence on phase shift, and developed a high-precision multiple reflection interference method[19,20] for measuring EO coefficients in a wide wavelength range, effectively eliminating the need for application of AR film.

This paper outlines the basics of the multiple reflection interference method and presents the values of the EO coefficients for non-doped CLN crystals, 5% MgO-doped CLN crystal and 1.8% MgO-doped quasi-stoichiometric LN (QSLN) crystal obtained by applying that method. Furthermore, the relationship between the manufacturing errors of the crystal and the precision of the measurement is reported.

2. Measurement Principle

As shown in Fig. 1, the multiple reflection interference method, which employs crystal-internal multiple reflection for the measurement of EO coefficients, makes use of an extremely simple optical system whereby a laser beam is incident normally on the parallelly polished faces of EO

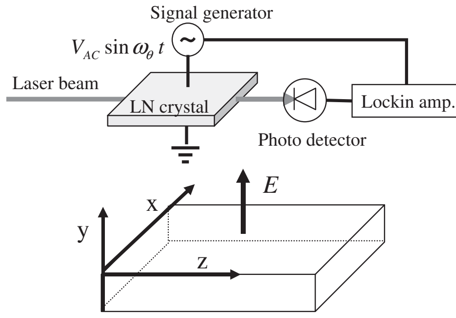

Fig. 1. Schematic arrangement for measuring the EO coefficient of LN crystal.

crystal. The EO coefficient of the sample is obtained from the interference between the light which passes through the crystal without being reflected and the light which passes through after being reflected multiple times inside the crystal.

In order to obtain precise dispersion of the EO coefficient, it is desirable that the phase variation for the multiply-reflected light be measured by consistently applying a single method. However, as shown in Table 1, the value of r_{22} of LN crystals for $\lambda = 632.8$ nm lies between 6.3 and 6.8 pm/V, with even lower values expected for the near-IR domain. As a consequence, both the highly precise domain null method in the 409–1064 nm range and the highly sensitive domain amplitude comparison method in the near-IR, which is characterized by low phase variation, have been used for the purposes of the present research. Details of each method are mentioned below.

2.1 Null method

As shown in Fig. 2, part of the linearly polarized laser light passes unobstructed through the LN crystal, while the remaining light passes after being reflected multiple times inside the crystal. Taking ω as the angular frequency of the laser light, $V_{AC}\sin\omega_\theta t$ as the alternating current applied to the crystal and R as the power reflectance of the faces of the crystal, the power I of the light passing through after bouncing $m + 0.5$ times can be expressed as follows:[3)]

$$I = \left\{ \sum_{k=0}^{m} R^k \sin[\omega t + (2k+1)(\theta\sin\omega_\theta t + \phi)] \right\}^2, \quad (1)$$

where ϕ is the static phase and $\theta\sin\omega_\theta t$ is the dynamic phase induced by the application of alternating current voltage. Each phase is induced by the light passing once through the

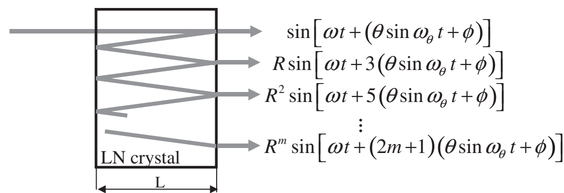

Fig. 2. Multiple reflections of light in the crystal at normal incidence.

insides of crystal. Expanding eq. (1) in a Bessel–Fourier series and letting P_m be the fundamental component signal with frequency identical to that of the applied voltage yields the following equation:

$$P_m = -2\sum_{l=0}^{m-1}\sum_{k=1}^{m-l} R^{k+2l}\sin(2k\phi)J_1(2k\theta)\sin\omega_\theta t, \quad (2)$$

where J_1 is a first-order Bessel function. Although eq. (2) includes two variables, ϕ and θ, it can be reduced to a function of θ by determining ϕ as described in ref. 20. In this case, choosing θ to be such that P_m becomes 0,[20)] the EO coefficient r_{22} of the LN crystal can be obtained from eq. (3). By taking L as the length and D as the thickness of the crystal, λ as the wavelength of the laser light and n_o as the normal refraction index for wavelength λ, θ can be found from the following equation:

$$\theta = \frac{\pi n_o^3 r_{22} L V_{AC}}{\lambda D}. \quad (3)$$

The highly accurate EO coefficient is obtained from the value of the voltage for which the fundamental component of the signal from the detector is at minimum.

2.2 Amplitude comparison method

The above mentioned null method produces high-precision results, however, the need for applying AC with amplitude larger than half wavelength voltage renders this method unusable whenever the EO coefficient of the crystal is small or IR light is employed for the measurement. In such cases, the amplitude comparison method is applicable.[17)]

In the amplitude comparison method, the EO coefficient is obtained from the amplitude ratio of the fundamental component P_m and the third harmonic component P_m^T. P_m^T is represented by the following equation:

$$P_m^T = -2\sum_{l=0}^{m-1}\sum_{k=1}^{m-l} R^{k+2l}\sin(2k\phi)J_3(2k\theta)\sin 3\omega_\theta t. \quad (4)$$

The amplitude ratio P_m/P_m^T can be expressed in the following manner:

$$\frac{P_m}{P_m^T} = \frac{\sum_{l=0}^{m-1}\sum_{k=1}^{m-l} R^{k+2l}\sin(2k\phi)J_1(2k\theta)}{\sum_{l=0}^{m-1}\sum_{k=1}^{m-l} R^{k+2l}\sin(2k\phi)J_3(2k\theta)}. \quad (5)$$

Equation (5) includes two variables, ϕ and θ, however, it can be reduced to a function of the variable θ by employing the same technique for determining ϕ as in the case of the null method. This function depends on the reflectance R. The relationship between the dynamic phase θ measured in $\lambda = 632.8$ nm for non-doped CLN crystals and the amplitude ratio $\alpha = P_m/P_m^T$ is shown in Fig. 3. Measuring the amplitude ratio α, the dynamic phase θ_β induced by the AC voltage V_{AC} can be determined from this figure. The r_{22} coefficient can be obtained by substituting those values in eq. (3).

The EO coefficient can be measured with much lower voltage by this method than that by the null method.

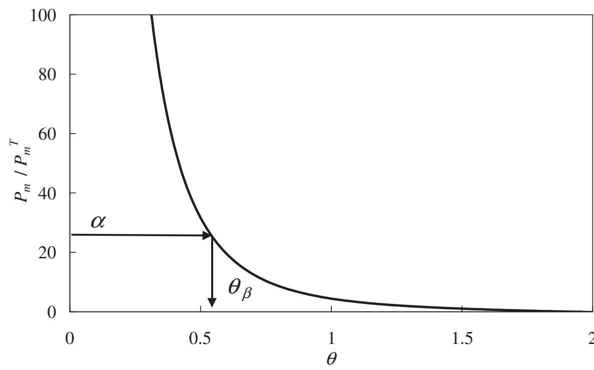

Fig. 3. θ_β is provided from measured value $\alpha = P_m/P_m^{\mathrm{T}}$.

Table 2. LN crystals dimensions and certified axial accuracy.

		Non-doped CLN	5% MgO-doped CLN	1.8% MgO-doped QSLN
LN crystal length (mm)	L	20.01	20.07	9.93
	d	2.00	2.00	2.00
Certified axial accuracy (deg)	X axis	<0.1	<0.1	<0.1
	Y axis	<0.1	<0.1	<0.1
	Z axis	<0.01	<0.01	<0.01

However, since the third harmonic component of the interference signal is very small for low voltage, the influence of electrical noise becomes considerable, which causes the relatively lower precision of this method in comparison with the null method.

3. Measurement Results

The LN crystal must be finely processed in the direction of each crystallographic axis in order to obtain a precise value of r_{22}. If the direction of the applied electric field and the direction of transmission of the light are not parallel to the crystallographic axes, the r_{13}, r_{33}, and r_{51} as well as the piezoelectric constants d_{13}, d_{33}, and d_{51} can influence the measurement value of r_{22}. The axial precision of the LN crystal was measured with an X-ray monocrystal orientation detector 2991F2 (Rigaku). All crystals used for the measurements had axial precision of less than 0.1° for the X axis, less than 0.1° for the Y axis, and less than 0.01° for the Z axis. The influence of those errors on the measurement results will be discussed in the next section. The size of the crystals was determined using image measurement system NEXIV VM-150M (Nikon). The sizes of all crystals used for the purpose of this experiment together with their respective axial precisions are shown in Table 2.

A detailed system diagram for the multiple reflection interference experiment is given in Fig. 4. The items of laser equipment for each wavelength are given in Table 3. The polarized direction of the laser was parallel to the X axis of the crystal. The reasons for preferring X to Y axis will be discussed in the next section. Exposure to a laser with wavelength shorter than that of blue light can cause optical damage to LN crystals. To avoid such damage, the intensity

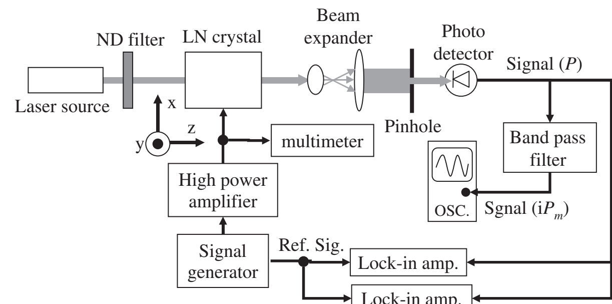

Fig. 4. Schematic arrangement for measurement by the amplitude comparison method of the EO coefficient of the LN crystal.

Table 3. Laser equipment specifications.

λ (nm)	Laser equipment
409	GaN laser
441.6	He–Cd laser
488, 515	Ar laser
543.5	
594.1	He–Ne laser
632.8	
700–900	Ti–Sa laser
1064	Nd:YAG laser
1340	Nd:YAP laser
1480–1580	InGaAsP laser

of the laser beam cast on the crystal was reduced to less than 10 µW by neutral density (ND) filters. Furthermore, the dynamic and static phases of the laser light were controlled by applying both AC voltage $V_{\mathrm{AC}} \sin(\omega_\theta t)$ and DC voltage V_{DC} to the crystal. The signal P from the detector was divided into three, one of which was passed through a band-pass filter with a central angular frequency set to ω, and the output signal P of the band-pass filter was observed with an oscilloscope. The fundamental component P_m and the amplitude of the third harmonic component P_m^{T} of P were measured by inputting each of the signals into two lock-in amplifiers.

The above measurements were carried on in a wavelength range from 409 to 1580 nm, and the dispersion of the r_{22} EO coefficients of non-doped CLN, 5% MgO-doped CLN, and 1.8% MgO-doped QSLN were obtained. The null method was applied to the 409–1064 nm domain, while the amplitude comparison method was applied to the 1340–1580 nm domain. The refractive indices n_{o} for non-doped CLN, 5% MgO-doped CLN, and 1.8% MgO-doped QSLN were obtained using the refractive index dispersion formulae of Edwards,[21] Shen *et al.*,[3] and Nakamura *et al.*,[1] respectively. Since the formula for the refractive index of QSLN as given by Nakamura *et al.* is based on measurement values in the 440–1050 nm wavelength, it can be assumed that the values of r_{22} for 409 and 1340–1580 nm are slightly erroneous.

Table 4 summarizes the measurement results of the r_{22} for non-doped CLN, 5% MgO-doped CLN, and 1.8% MgO-doped QSLN. Those values represent the average result from

Table 4. Measurement results.

λ (nm)	Non-doped CLN		5% MgO-doped CLN		1.8% MgO-doped QSLN	
	n_o	r_{22} (pm/V)	n_o	r_{22} (pm/V)	n_o	r_{22} (pm/V)
409	2.4256	9.58	2.4186	9.40	2.4280	9.90
441.6	2.3870	8.85	2.3804	8.59	2.3842	9.27
488	2.3486	8.03	2.3426	7.79	2.3459	8.41
515	2.3321	7.62	2.3264	7.33	2.3296	8.04
543.5	2.3177	7.29	2.3123	6.94	2.3156	7.63
594.1	2.2980	6.80	2.2930	6.44	2.2962	7.18
632.8	2.2864	6.54	2.2816	6.20	2.2849	6.97
700	2.2710	6.23	2.2666	5.85	2.2689	6.64
750	2.2623	6.09	2.2580	5.72	2.2612	6.50
800	2.2553	5.93	2.2509	5.56	2.2542	6.34
850	2.2494	5.73	2.2450	5.40	2.2484	6.21
900	2.2444	5.59	2.2399	5.24	2.2433	6.13
1064	2.2322	5.45	2.2272	5.12	2.2307	5.97
1340	2.2189	5.23	2.2124	5.00	2.2156	5.82
1480	2.2137	5.16	2.2062	4.89	2.2092	5.74
1510	2.2126	5.15	2.2049	4.83	2.2080	5.73
1550	2.2112	5.13	2.2032	4.82	2.2062	5.72
1580	2.2102	5.12	2.2020	4.80	2.2049	5.71

10 measurements. The standard deviation for these data is approximately 0.02 pm/V in the case of the null method, and approximately 0.05 pm/V in the case of the amplitude comparison method. Using these results, the coefficients *A*–*E* in eq. (6), and chi square values, and R-square value were obtained, and the wavelength dispersion equation for r_{22} in the 409–1580 nm wavelength was derived:

$$r_{22}(\lambda) = A + \frac{B}{\lambda^2 - C} + \frac{D}{\lambda^2 - E} \quad (\lambda\text{: µm}). \tag{6}$$

Table 5 gives the values of each constant for each respective crystal. The half wavelength voltage for each crystal was calculated from the above results by employing the following equation:

$$V_\pi = \frac{\lambda D}{n_o^3 r_{22} L}. \tag{7}$$

The values of the half-wavelength voltage for each crystal are given in Table 6. Figures 5–7 represent the relationship between the wavelength and the measurement values with a fitting curve calculated from wavelength dispersion equation, as well as the relationship between the wavelength λ and the half wavelength voltage V_π. Here, the following equation can be derived by partial differentiation of eq. (7) with respect to the wavelength:

$$\frac{\partial V_\pi}{\partial \lambda} = \frac{D}{n_o^3 r_{22} L}\left(1 - \frac{3\lambda}{n_o}\frac{\partial n_o}{\partial \lambda} - \frac{\lambda}{r_{22}}\frac{\partial r_{22}}{\partial \lambda}\right). \tag{8}$$

It can be inferred from the above equation that the slope of V_π becomes smaller as λ become larger. From Figs. 5–7, we can see the slightly non-linear nature of V_π.

4. Influence of Manufacturing Error of LN Crystal on Measurement Results

Regardless of how carefully the crystal is manufactured, the normals to the faces of the crystal and its optical axes can

Table 5. Coefficients of the wavelength dispersion equation, and chi-square value and *R*-square value for r_{22} at 25 °C.

	Non-doped CLN	5% MgO-doped CLN	1.8% MgO-doped QSLN
A	4.90788	4.55966	5.61263
B	1.02070	0.47994	1.59123
C	0.00764	0.04544	−0.02394
D	−0.49417	0.11774	−1.37924
E	−0.12470	0.04544	−0.17910
χ^2	0.00212	0.00448	0.00171
R^2	0.99912	0.99821	0.99921

Table 6. Calculated half-wave voltage.

λ (nm)	Half-wave voltage (V)		
	Non-doped CLN	5% MgO-doped CLN	1.8% MgO-doped QSLN
409	149.6	153.8	292.1
441.6	183.5	190.6	355.7
488	234.7	243.7	454.9
515	266.4	279.1	512.9
543.5	299.5	316.8	580.6
594.1	360.0	382.7	691.7
632.8	404.8	429.8	770.4
700	479.5	514.0	913.7
750	532.1	569.7	1009.5
800	588.6	631.1	1114.9
850	652.1	695.9	1219.8
900	712.2	764.4	1316.8
1064	878.0	940.8	1625.2
1340	1172.1	1237.8	2142.6
1480	1322.6	1409.8	2420.4
1510	1353.9	1458.8	2477.8
1550	1397.8	1504.0	2554.1
1580	1429.6	1542.1	2612.7

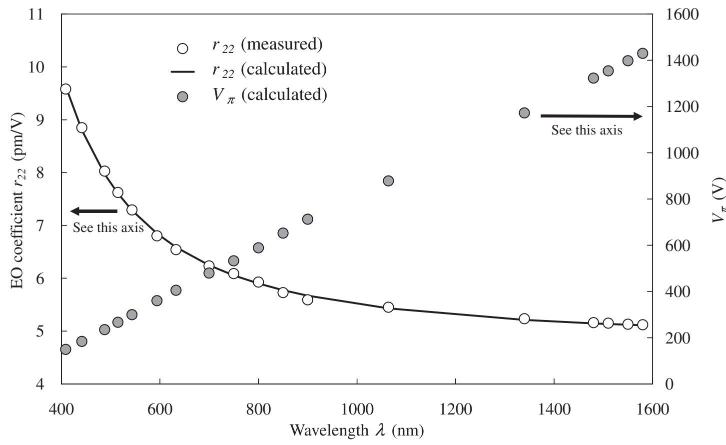

Fig. 5. Wavelength dependence of r_{22} and half wave voltage at 25 °C (non-doped CLN).

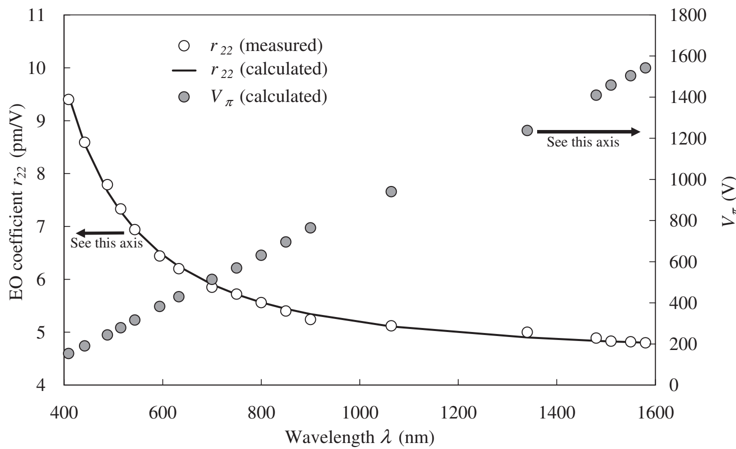

Fig. 6. Wavelength dependence of r_{22} and half wave voltage at 25 °C (5% MgO-doped CLN).

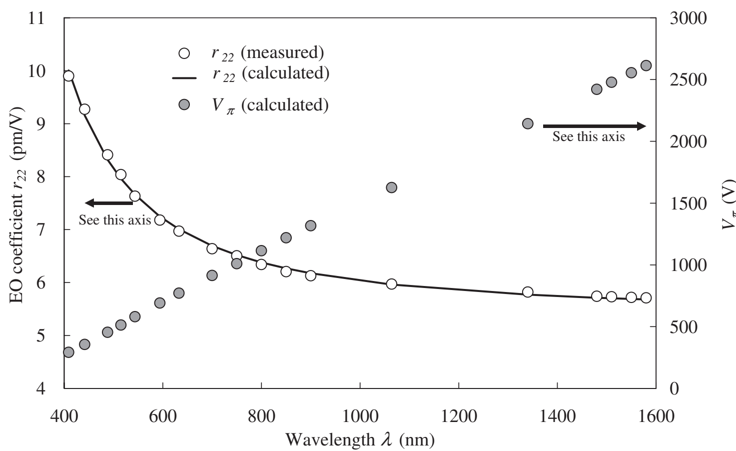

Fig. 7. Wavelength dependence of r_{22} and half wave voltage at 25 °C (1.8% MgO-doped QSLN).

never be made to coincide. Due to manufacturing imperfections, other coefficients such as r_{13}, r_{33}, r_{51}, d_{15}, d_{31}, or d_{33} may contribute to the measurement value of r_{22}. This influence will be discussed in this section. One of our authors has clarified the dependency between the changes in the refractive index and the EO coefficient of LN crystals, as well as the relationship between the length change of the crystal and the dynamic phase θ, induced by inverse piezoelectric effect.[22] In this section, we discuss the relationship between the manufacturing error and the measurement errors with respect to the above effects.

X', Y', and Z', as shown in Fig. 8, designate the normals to the faces of the optically polished LN crystal. Here X, Y, and Z are not perpendicular to each other. For the purposes of calculational simplicity, one of those three axes has been assumed to be the crystallographic axis of the crystal. This means, in Fig. 8, the crystallographic axis X and the normal X' coincide, while Y and Y', Z and Z' intersect at the angle η and ξ, respectively. If Z' is the direction of propagation of the light and Y' is the direction of the applied electrical field as illustrated in Fig. 8, the EO coefficients $r_{X'}$ and $r_{Y'}$, involved in the phase of light linearly polarized along the

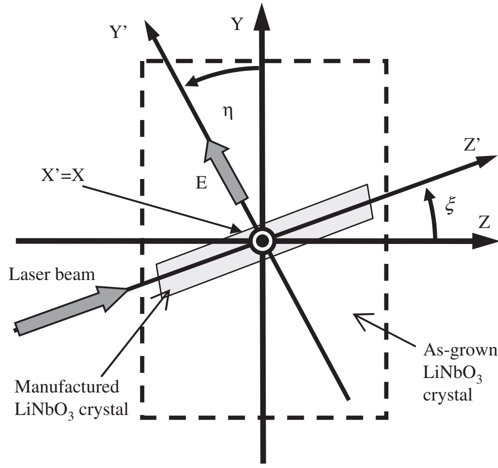

Fig. 8. Crystal orientation of LiNbO$_3$ crystal.

direction of X' $(=X)$ and Y', can be obtained from the following equations:

$$r_{X'} = -(-r_{22}\cos\eta + r_{13}\sin\eta), \quad (9)$$

$$r_{Y'} = -(r_{22}\cos\eta\cos^2\xi + r_{13}\sin\eta\cos^2\xi + r_{33}\sin\eta\sin^2\xi + 2r_{51}\cos\eta\cos\xi\sin\xi). \quad (10)$$

The piezoelectric constant $d_{z'}$, related to the expansion and contraction of the crystal, can be expressed as:

$$d_{Z'} = (d_{22}\cos\eta + d_{31}\sin\eta)\sin^2\xi - 2d_{15}\cos\eta\sin\xi\cos\xi + d_{33}\sin\eta\cos^2\xi. \quad (11)$$

Furthermore, the following equation gives the effective refractive index n_{oe}, affecting the light polarized along the direction of Y':

$$n_{\mathrm{oe}} = \frac{n_{\mathrm{e}}}{\sqrt{\sin^2\xi + (n_{\mathrm{e}}/n_{\mathrm{o}})^2\cos^2\xi}}. \quad (12)$$

Therefore, taking the EO and the piezoelectric effects into consideration, the effective EO coefficients $r^{\mathrm{E}}_{X'}$ and $r^{\mathrm{E}}_{Y'}$ in the direction of X' and Y' can be obtained in the following equations:

$$r^{\mathrm{E}}_{X'} = r_{X'} + \frac{2}{n_{\mathrm{o}}^2}d_{Z'}, \quad (13)$$

$$r^{\mathrm{E}}_{Y'} = r_{Y'} + \frac{2}{n_{\mathrm{oe}}^2}d_{Z'}. \quad (14)$$

The value of the effective EO coefficients obtained from eqs. (13) and (14) in the direction of X' and Y' is shown in Fig. 9. Figure 10 outlines the results of the effective EO coefficients in the direction of X' and Y' when Y and Y' coincide, while X and X', Z and Z' intersect at the angle ψ and ξ, respectively. In both cases, the following values were used in conducting the calculations: $r_{13} = 9.6$ pm/V, $r_{33} = 30.9$ pm/V, $r_{51} = 32.6$ pm/V, $d_{15} = 74.0$ pC/N, $d_{31} = -0.86$ pC/N, $d_{33} = 16.2$ pC/N.[23] Furthermore, the measurement value of 6.54 pm/V was used for r_{22}. In case each of the rotational angles η and ξ of the crystal deviates by $\pm 0.1°$, the fluctuation margin of $r^{\mathrm{E}}_{X'}$ is approximately $\pm 1.9\%$, while the fluctuation margin of $r^{\mathrm{E}}_{Y'}$ is approximately $\pm 3.4\%$. Therefore, it has become clear that high precision measurements of the r_{22} of LN crystals can be conducted by setting the laser polarized along X' axis. This result derives from the fact that the $2r_{51}\cos\eta\cos\xi\sin\xi$ term in eq. (10) exerts stronger influence on $r^{\mathrm{E}}_{Y'}$ than that on $r^{\mathrm{E}}_{X'}$.

Since the Z axial accuracy of the sample crystals is less than $\pm 0.01°$, the rotational angles η and ξ are less than $\pm 0.01°$. Thus, it can be concluded from Figs. 9–10 that the influence of the manufacturing error of the r_{22} is less than approximately 0.1%.

5. Conclusion

The EO coefficient r_{22} for several types of LN crystal under constant stress conditions was measured for 409–1580 nm by the multiple reflection interference method. This is the first time that the r_{22} dispersion equation has been obtained for such a wide wavelength interval. We also discussed the influence of manufacturing errors on the measurement results. Regarding this influence, the experimental errors are less than approximately 0.5% for the null method and approximately 1% for the amplitude comparison method. It further became clear when the laser was polarized along X axis, the measurement of the r_{22} of LN crystals will

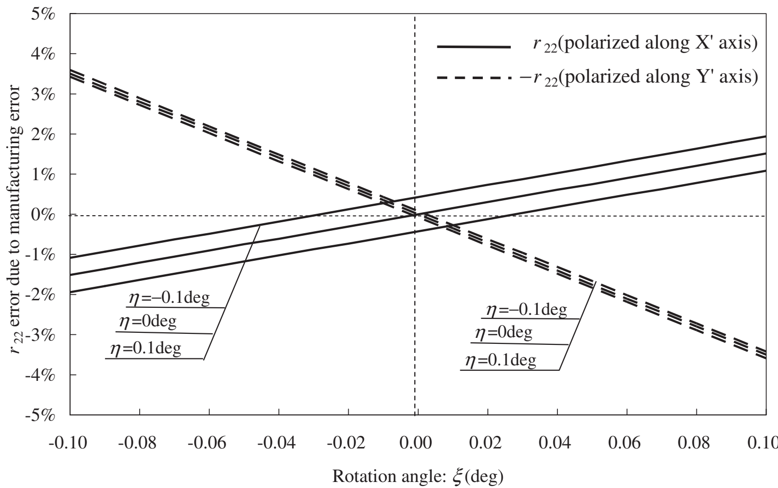

Fig. 9. Influence of η and ξ to measurement results of EO coefficients r_{22} (X') and r_{22} (Y') when X and X' coincide.

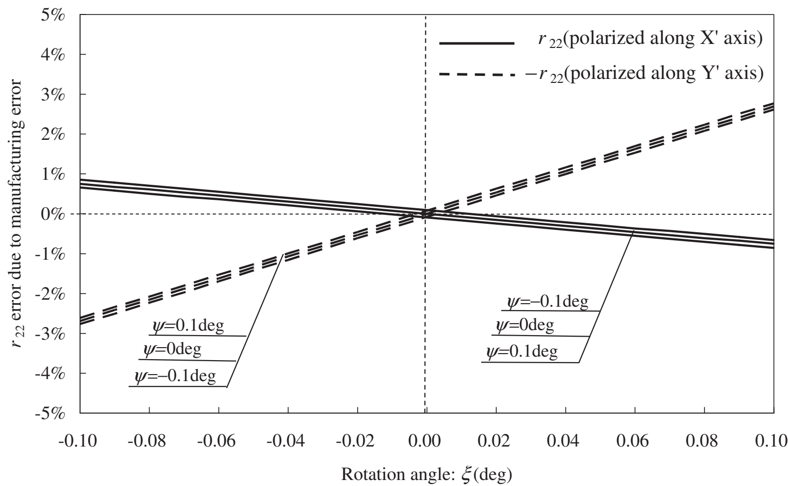

Fig. 10. Influence of η and ξ on measurement results of EO coefficients r_{22} (X') and r_{22} (Y') when Y and Y' coincide.

have high accuracy. This method is able to be used for future measurements of any EO coefficients of any EO crystals.

Acknowledgements

This research was supported by a Grant-in-Aid for Creative Scientific Research 2002–2006 and "High-Tech Research Center" Project for Private Universities: matching fund subsidy from Ministry of Education, Culture, Sports, Science and Technology (MEXT), 2002–2006, of Japan, for which we express gratitude. In addition, we have had fruitful discussion about handling of infrared laser and detector with Drs. Y. Suzuki, M. Doshida, and K. Ota from Technical Research and Development Institute, Ministry of Defense.

References

1) M. Nakamura, S. Higuchi, S. Takekawa, K. Terabe, Y. Furukawa, and K. Kitamura: Jpn. J. Appl. Phys. **41** (2002) L49.
2) F. Abdi, M. Aillerie, P. Bourson, M. D. Fontana, and K. Polgar: J. Appl. Phys. **84** (1998) 2251.
3) H. Y. Shen, H. Xu, Z. D. Zeng, W. X. Lin, R. F. Wu, and G. F. Xu: Appl. Opt. **31** (1992) 6695.
4) R. K. Choubey, P. Sen, R. Bhatt, S. Kar, V. Shukla, and K. S. Bartwal: Opt. Mater. **28** (2006) 467.
5) E. Kraetzig and H. Kurz: J. Mod. Opt. **24** (1977) 475.
6) S. Kawada: O plus E **201** (1996) 72.
7) V. B. Markov, Y. N. Denisyuk, and R. Amezquita: Opt. Mem. Neural. Netw. **6** (1997) 91.
8) R. Grousson and S. Mallick: Appl. Opt. **19** (1980) 1762.
9) T. Kawanishi, T. Sakamoto, S. Shinada, M. Izutsu, K. Higuma, T. Fujita, and J. Ichikawa: Electron. Lett. **40** (2004) 691.
10) M. Doi, M. Sugiyama, K. Tanaka, and M. Kawai: IEEE J. Sel. Top. Quantum Electron. **12** (2006) 745.
11) K. Onuki, N. Uchida, and T. Saku: J. Opt. Soc. Am. **62** (1972) 1030.
12) Y. Fujii and T. Sakudo: J. Appl. Phys. **41** (1970) 4118.
13) J. Zook, D. Chen, and G. Otto: Appl. Phys. Lett. **11** (1967) 159.
14) H. Y. Zhang, X. H. He, Y. H. Shin, and S. H. Tang: Opt. Commun. **86** (1991) 509.
15) M. Aillerie, M. Fontana, F. A. C. Carabatos-Nedelec, N. Theofanous, and G. Alexakis: J. Appl. Phys. **65** (1989) 2406.
16) M. Abarkan, J. P. Salvestrini, M. Aillerie, and M. D. Fontana: J. Appl. Phys. **42** (2003) 2346.
17) K. Takizawa and Y. Yokota: Opt. Rev. **13** (2006) 161.
18) A. Chirakadze, S. Machavariani, A. Natsvilishvili, and B. Hvitia: J. Phys. D **23** (1990) 1216.
19) K. Takizawa and M. Okada: J. Opt. Soc. Am. **72** (1982) 809.
20) K. Yonekura, L. Jin, and K. Takizawa: IEICE Trans. Electron. **J89-C** (2006) 1124 [in Japanese].
21) G. J. Edwards: Opt. Quantum Electron. **16** (1984) 373.
22) K. Takizawa: Appl. Opt. **42** (2003) 1052.
23) *Numerical Data and Functional Relationships in Science and Technology*, ed. K. H. Hellwege (Springer, Berlin, 1979) Landolt-Börnstein New Series, Group III, Vol. 11, pp. 390, 552.
24) P. V. Lenzo, E. G. Spencer, and K. Nassau: J. Opt. Soc. Am. **56** (1966) 633.
25) P. H. Smakula and P. C. Claspy: Trans. Metall. Soc. AIME **239** (1967) 421.
26) F. Abdi, M. Aillerie, P. Bourson, M. D. Fontana, and K. Polgar: J. Appl. Phys. **84** (1998) 2251.
27) H. Iwasaki, H. Toyoda, N. Niizeki, and H. Kubota: Jpn. J. Appl. Phys. **6** (1967) 1419.